

Girão-Coelho AM, Mottram JT, Matharu N. [Virtual characterization of delamination failures in pultruded GFRP angles](#). *Composites Part B: Engineering* 2016, 90, 212-222.

**Copyright:**

© 2016. This manuscript version is made available under the [CC-BY-NC-ND 4.0 license](#)

**DOI link to article:**

<http://dx.doi.org/10.1016/j.compositesb.2015.12.025>

**Date deposited:**

26/01/2016

**Embargo release date:**

07 January 2017



This work is licensed under a [Creative Commons Attribution-NonCommercial-NoDerivatives 4.0 International licence](#)

# Virtual characterization of delamination failures in pultruded GFRP angles

Ana M. Girão Coelho

Lecturer (former Marie Curie IEF Research Fellow at the University of Warwick)  
(Corresponding author, [ana.girao-coelho@ncl.ac.uk](mailto:ana.girao-coelho@ncl.ac.uk))  
School of Engineering and Geosciences, Newcastle University, Newcastle upon Tyne, NE1 7RU, UK

J. Toby Mottram

Professor  
([j.t.mottram@warwick.ac.uk](mailto:j.t.mottram@warwick.ac.uk))  
School of Engineering, University of Warwick, Coventry CV4 7AL, UK

Navroop Matharu

Civil Engineer  
([navroop.matharu@hyderconsulting.com](mailto:navroop.matharu@hyderconsulting.com))  
Hyder Consulting (UK) Ltd, Birmingham B6 5RQ, UK

---

## Abstract

This paper deals with the application of cohesive zone models to study delamination failures in leg-angles of pultruded glass fibre reinforced polymer material using the general-purpose finite element software Abaqus. The objective of the study is present a finite element modelling methodology that can, for example, help to fill-in knowledge gaps in the available experimental data pertaining to the tying force resistance of angle-cleated jointing in frame construction. It may be used to optimize cleat shape and laminate lay-up (dependent on composite processing method) for the strongest cleat against a minimum cost requirement. A benchmark example taken from literature is used to show that the numerical predictions from the authors' simulations are reliable. The approach is next used to analyse an equal leg-angle component where one leg is fixed and the other orthogonal leg is being deformed by a tensile force applied over the free end surface. Numerical results from Abaqus are used to show that a lamination produced by the pultrusion processing method fails unstably by delamination cracks radiating around the curved region and extending into the leg panels. As a preliminary study to show the potential of the new modelling methodology it is used to show the influence of the radius of curvature at the junction between the legs on the tying force resistance; based on the load at delamination onset a smaller radius reduces the cleat's strength.

*Authors Keywords:* Curved laminates; Delamination; Finite element analysis; Damage mechanics; Pultruded GFRP material

---

# 1. Introduction

Pultruded Glass Fibre Reinforced Polymer (GFRP) shapes and systems are becoming recognized as an attractive primary structural material in low-rise building residential and commercial constructions owing to an overall property portfolio that is favourable for achieving sustainable, low carbon construction [1]. Pultrusion is an economical way of producing constant thin-walled shapes of FRP laminated composite material. Standard GFRP shapes consist of glass fibre reinforcement (layers of UniDirectional (UD) rovings and mat) in a thermoset (typically, polyester or vinylester) resin based matrix. Their standard shapes resemble counterparts found in structural steelwork, and depending on laminae construction they have direct strengths in the longitudinal direction of 200 to 400 N/mm<sup>2</sup>. The strengths in the transverse direction are one third of the longitudinal values and maybe lower again in the through-thickness direction. The modulus of elasticity along the length lies in the range from 20 to 30 GPa, in transverse direction from 6 to 10 GPa and the in-plane shear modulus between 3 to 5 GPa. Mechanical properties will depend on constituent properties, the pultrusion composite processing conditions and long-term loading and environmental actions.

Arguably, one of the key barriers to wider exploitation of this construction material (like steel, concrete and timber) is the lack of reliable methods for the prediction of emergence and growth of composite-specific failure modes, especially from delamination where cracks initiate and grow between the lamination layers. In this paper the meaning of the word *crack* is synonymous with the meaning of *fracture*. While physical testing should provide the most reliable information about the load-carrying behaviour of GFRP materials, members, sub-assemblies and structures, numerical (virtual-prototyping) tests will provide insight into the mechanics involved in the structural behaviour. Advanced computational analysis has the capability of representing with extreme numerical accuracy the onset and progression of delamination between the laminae. Girão Coelho [2] has discussed the difficulties to be overcome when developing numerical formulations capable of predicting the delamination dominated failure. Only flat plate laminate configurations, where delamination growth is stable, were then considered.

This is not the case with pultruded GFRP shapes (e.g. I, H, leg-angle) that have a web-flange or leg curved junction, which is a non-flat configuration where delamination growth is to be unstable or changes from unstable to stable, depending on the localized deformations. A representative example of such configurations is the case of an equal-leg angle profile subjected to tensile loading applied uniformly through one leg and in this leg's plane, whilst the other leg is: (i) totally restrained [3]; (ii) has a bolted connection with two or three bolts across a single bolt row, usually at the mid-distance for the leg's length. [4]. Because angle profiles are used as connecting components in

framed joints (for bolted connections refer to introduction in [4]), and with the concept of robustness and structural integrity being given thoughtful consideration, research into the delamination problem in GFRP angles subjected to tensile loading (known as tying force) is timely.

Finite Element (FE) simulations as virtual tests are performed in this current work at the mesoscale level of the structural composite to evaluate the tying force resistance. Each lamina in the GFRP leg-angle is modelled as a homogeneous, anisotropic continuum and a relative very thin resin layer (quantified later) is assumed to contain any delamination cracking between stacked layers. A cohesive zone model is implemented to predict the size and position of the initial delamination, as well as the load-carrying capacity of the deforming leg-angle. In this paper the word *delamination* has the meaning for the formation and growth of a flat flaw in an initially flawless interface (between two laminae) that grows into a sizeable delamination crack.

The paper begins by describing the cohesive zone modelling approach to treat delamination in laminated composite components. Presented next are results from material coupon testing with the Pultex® SuperStructural Series 1525 GFRP material (that is for the leg-angles used in the tying force experimental programme reported in [4]). The virtual test approach used to simulate the physical testing is then described and numerical results are presented and discussed. The effect of changing the curvature at the leg-angle (right-angle) junction when determining the tying force strength is introduced. Conclusions are finally drawn and further research is suggested.

## **2. Fundamental behaviour and analysis approach**

Delamination cracks are often seen to occur at stress free edges due to the mismatch in directional properties of the individual fibre reinforced laminae, at notches or at curved regions of composite components, such as found in the engineering problem that is the subject of this numerical investigation. This paper is specifically concerned with having a pair of web cleats connecting a beam to a column member for a beam-to-column joint [4] that is subjected to tension loading with an action direction coinciding with the longitudinal centroid of the beam's cross-section. This specific load case is important should the column member become discontinuous below the level of the joint and the upper level of cleating has to support the floor loading, via catenary action in the suspended beam members [4]. Due to the curvature in the cleat components there are in this region to be high normal stresses in the out-of-lamina direction. Such angles of GFRP thus represent a potential zone of weakness in pultruded framed structures. The delamination-induced damage in the root of an angle

subjected to a tying force is a potential source of failure that has not been addressed previously, specifically in terms of advanced computational analysis.

The aim of this paper is to develop a FE approach that will characterize the delamination-dominated failures in the critical regions of pultruded GFRP cleats under representative static loading. This work is supplemented by having results to compare with from a series of physical tests carried out by Qureshi *et al.* [4]. In the present study, the numerical models include a continuum damage approach to intralaminar failure modelling and a cohesive zone model to represent the delamination behaviour at the laminae interfaces. When properly implemented, this approach ensures a large degree of objectivity with respect to FE discretization and requires little or no modification to standard commercial FE codes, such as the general purpose software Abaqus [5]. This latter aspect is particularly relevant to practicing engineers concerned with virtual testing related to structural integrity and damage tolerance of composite structures for safety-critical structures.

In most structural building codes there are specific integrity requirements in order to avoid disproportionate collapse [6,7]. *Disproportionate collapse* can be defined as a region of structural collapse out of proportion to the initiating cause of failure. The most relevant to connection/joint design is that the detailing for every beam member must possess a minimum horizontal force at ultimate failure (or *tying resistance*). Tying force requirements and their implications to design and detailing (these are for the design of steel frames usually simple rules that will enhance general structural integrity and provide greater resistance to disproportionate collapse). Background information on this important basic design requirement towards safe and reliable pultruded framed structures is given in what follows.

### 2.1. Modelling of progressive delamination using cohesive zone models

FRP materials used in structural engineering combine reinforcing fibres and polymer resin based matrix. The fibres provide the high stiffness and strengths, while the surrounding matrix holds the composite together. The fibre-matrix interphase (or interface) consists of a bond region of a few nanometres thickness between fibre and bulk matrix and the immediate adjacent region. The load transfer from matrix into fibres that takes place at the interphase layer is primarily a mechanistic process and involves the interfacial bond and friction. Delamination is defined as the separation of reinforcing layers from each other, as a consequence of shear stresses acting in planes parallel to the layers interfaces and/or tensile stresses acting in the through-thickness direction. This phenomenon is a typical *crack growth* problem and is treated in the framework of fracture mechanics. Today, the most popular computational method for the prediction of delamination

failure is based on *cohesive zone models* that provide a natural bridge between strength-based models and energy-based models for fracture. This allows delamination to be described by a single framework that covers a range of applications for which a strength or an energy criterion alone might not be sufficient.

Cohesive zone models consider fracture as a gradual phenomenon in which separation takes place across an extended crack tip, or cohesive zone, and is resisted by cohesive tractions [8-10]. Thus cohesive zone elements do not represent any physical material, but describe the cohesive forces which occur when layers in a laminated material are being pulled apart. In FE modelling, cohesive zone elements are placed between the continuum elements used to model the layers. A key analysis feature of these elements is that they include the effect of first failure, and the subsequent crack propagation by means of critical strain energy release rates.

The simulation of interlaminar damage for delamination failure will be based on the cohesive zone approach using the Abaqus three-dimensional cohesive element COH3D8. The study is performed in the quasi-static regime. The traction-separation law formulation assumes a non-zero elastic stiffness of the cohesive zone, which is physically motivated by the reduced stiffness of the matrix-rich very thin interface layer as compared to a perfect bond assumed to exist between fibres and matrix in layer. From a numerical point of view, this elastic stiffness can be understood as a penalty-type enforcement of displacement continuity in the elastic range.

A quadratic stress criterion is used for the damage initiation criterion. To specify the conditions for separation in the cohesive zone model [11-13] the following expression is chosen:

$$\left(\frac{\langle \sigma_n \rangle}{f_I}\right)^2 + \left(\frac{\sigma_s}{f_{II}}\right)^2 + \left(\frac{\sigma_t}{f_{III}}\right)^2 = 1 \quad (1)$$

whereby  $\sigma_n$  is the stress in pure opening mode,  $\sigma_s$  is the stress in the first shear direction,  $\sigma_t$  is the stress in the second shear direction,  $f_I, f_{II}$  and  $f_{III}$  are the peak strength values in the same directions, and:

$$\langle \sigma_n \rangle = \sigma_n \quad \text{for } \sigma_n > 0 \quad \text{and} \quad \langle \sigma_n \rangle = 0 \quad \text{for } \sigma_n \leq 0 \quad (2)$$

because compressive normal stresses cannot open the delamination crack.

Progression of damage at the interfaces is modelled using a linear softening law and a critical mixed mode energy behaviour based on the Benzeggagh-Kenane criterion [14], which is described by the following expression:

$$G_c = G_{I,c} + (G_{II,c} - G_{I,c}) \left[ G_{II} / (G_I + G_{II}) \right]^\eta \quad (3)$$

$G_{m,c}$  (with  $m = I, II, III$ ) is the total critical strain energy release rate associated with delamination mode  $m$ , and  $\eta$  is the semi-empirical criterion exponent applied to delamination initiation and

growth. Illustrated in Figs. 1a to 1c are the three modes that can singular or interact to cause a delamination failure.

The use of cohesive zone models in FE analyses requires that a very fine mesh specification is used to ensure that sufficient interface elements exist within the cohesive zone length at the crack tip. If the mesh design happens to be too coarse, the cohesive stress at the discontinuity may not even reach the interfacial strength and, as a result, the required failure mode is missed. Falk *et al.* [15] suggest a minimum of two to five elements in this cohesive zone length in order to perform a reliable simulation. Turon *et al.* [16] indicate that for typical graphite-epoxy or glass-epoxy composite materials, the length of the cohesive zone should be smaller than one or two millimetres. As a consequence, the mesh size required in order to have more than two elements in the cohesive zone should be smaller than half a millimetre. For full-sized structural models of pultruded GFRP components and structures this has the obvious consequence of a computationally expensive solution. Current numerical simulations comply with the cohesive zone element mesh size requirements specified by the first author [2] to allow stable numerical simulations of interface delamination.

## 2.2. Design provisions for structural integrity of frame joints

Disproportionate collapse is a relatively rare event in Western nations, as it requires both an abnormal/accidental loading to initiate the local damage and a structure that lacks adequate continuity, ductility, *integrity*, *robustness* and *redundancy* to resist the spread of damage. Significant casualties can be the consequence when there is collapse of *key elements*. In this paper, the following terminology for the highlighted words (or concepts) is adopted [17]:

- *Integrity* is the ability of the elements of a structure to remain connected in the event that forces are applied beyond the design loads. Requiring connections between members to be designed for minimum tension forces are means of achieving structural integrity.
- *Robustness* is the ability of a structure or a structural element to resist forces beyond its design forces. Robustness of an overall structure can be achieved by strengthening individual members, by providing elements with high levels of energy absorption or by providing alternate means of support of a given area.
- *Redundancy* is the provision of alternate load paths (that have the capacity to resist the full design load) for a load applied at a specific location.
- *Key elements* (e.g. *joints* or *connections*) are structural elements that if they failed would cause the collapse of an unacceptable region in the structural system.

The European code EN 1991 [6] and the American standard SEI/ASCE [7] have specific structural integrity requirements for building structures in order to avoid disproportionate collapse, which, in general, specify that each beam connection must develop a minimum horizontal (axial) tension capacity, and each column splice has a minimum vertical tension capacity. These requirements do mandate the verification that connections develop minimum levels of tying resistance and can usually be met in most buildings with no cost implications and minimal calculations to verify compliance. For pultruded joints and connections, the ASCE pre-standard for Load and Resistance Factor Design (LFRD) of pultruded Fiber Reinforced Polymer (FRP) Structures [18] proposes a minimum horizontal tying force in the mandatory part. Section 2.9 [18] states, *“Notwithstanding the required connection strength determined from structural analysis, the design strength of structural connections shall not be less than 1 kip (4.5 kN). Should a column lose its continuity, below the locations where beams are connected, and the FRP clip angles are required to take tension action, to prevent disproportionate collapse...”*. In this paper the meaning of the word *connection* as used in ASCE [18] is *joint* since the Eurocode terminology is used. There is no provenance to the rationale for the target tying force being specified at 4.5 kN other than the test strength results in [3]. To know what the strength is of GFRP cleats in the field are is one research question that the numerical results from using the novel finite element modelling methodology presented in this paper can help to address.

### **3. Material properties of the Pultex® SuperStructural material**

This section describes the physical and mechanical properties of panel material in a pultruded GFRP leg-angle shape that is used in the experimental programme reported in [4] and for the comparison with FE results in Section 4. The fibre architecture and constituent properties are presented along with measured strengths and moduli of elasticity, and the later predicted on applying micromechanical modelling with known and assumed constituent properties. The purpose of this section is to introduce properties for the pultruded material required in the FE modelling to predict delamination failure and its progress when a leg-angle is subjected to tying force deformation.

The material is from Creative Pultrusions Inc., and the Pultex® SuperStructural 1525 series of ‘off-the-shelf’ shapes. Identifier number 1525 means the thermoset polyester matrix is Class 1 Flame Retardant. The colour of the material is Gray. It has been manufactured using traditional continuous pultrusion [19] with the addition of closed mould resin injection instead of an open resin



bath. This method is known to ensure there is an effective saturation of the resin matrix throughout the E-glass fibre reinforcement and generate less voiding [20].

### *3.1. Physical properties*

#### *3.1.1. Fibre reinforcement*

The equal leg-angle shape has a cross-section (75×75×9.6 mm) for a thin-walled section. Panels have a combination of fibre reinforcement in layers of UD rovings and a Tri-axial Stitched Fabric Mat (TSFM), as shown in Fig. 2. A photograph showing a panel's lay-up is seen in Fig. 2a with a close-up in Fig. 2b to show the fibre construction in a TSFM layer (product E-TTXM 4008 from Vectorply® corporation). As seen in Fig. 2a there are seven alternating layers of UD and TSFM, with two TSFM layers at mid-thickness. TSFM is of a stitched continuous fabric having four layers with the fibre lay-up sequence of +45°/90°/-45°/random Chopped Strand Mat (CSM). It is known from Creative Pultrusions Inc. that 56 yield rovings are used for the UD roving layers in the 9.6 mm thickness ( $t$ ). At both surfaces there is an outer (relatively thin) non-structural Surface Veil (SV) to provide UV protection and a barrier to moisture diffusion. The NEXUS® veil layer is resin-rich and consists of randomly orientated short 100% melt polyester fibres, which has a mass per unit area < 100 g/m<sup>2</sup> and a semi-glossy finish that allows the pultruded to be easily handled.

#### *3.1.2. Resin matrix*

The thermoset resin is the Reichhold 31031 unsaturated isophthalic (an isomer of phthalic acid benzene-1 and 3-dicarboxylic acid) polyester resin. To produce the matrix there are additives. The filler is clay, assumed to be aluminium silicate, which is commonly kaolin clay. This filler is used, in addition to economic purposes, to improve chemical resistance, opacity, surface finish, and insulation properties [21]. The Flame Retardant additive is antimony trioxide acts alongside the other resin base of brominated polyester to provide the 1525 series shapes with fire protection. Other additives include a mould releasing agent, and low, mid and high range catalysts activated during the pultrusion composite processing. Finally, internal stresses and cracking issues are dealt with the addition of glass beads. UV inhibitors are present in the additive design. The largest proportions in the matrix formula, which consist of 13 constituent parts, are for the polyester resin, known to be approximately 80% of the bulk matrix.

### 3.1.3. Constituent material properties

A series of resin burn-off tests were conducted to estimate the volumetric proportions of UD and TSFM fibres and matrix, as well as to establish the nominal thicknesses of each layer in a pultruded panel. The resin burn-off procedure was adapted from the method described in Appendix B of the PhD thesis by Lane [22], and with reference made to the testing procedure given in [23,24]. Table 1 summarizes the results from the resin burn-off tests. Because the reinforcing effect of the SV layers is minimal it can be seen that the total amount of glass fibre with the two main reinforcing types of UD and TSFM are equal. In the leg-angle the volume percentages of UD, TSFM and matrix are in the range 30 to 34. The final row in Table 1 reports the nominal thicknesses of the layers on the assumption that they are constants for a particular fibre reinforcement type.

## 3.2. Mechanical properties

The data presented for mechanical properties is defined with respect to the local material coordinate system, with: 1 for the UD fibre direction; 2 for the in-plane direction normal to UD fibres; 3 for the through-thickness direction. The normal direction is in the direction of pultrusion, and in the literature is often referred to as the longitudinal direction. Notation  $f_1$  is therefore for the in-plane longitudinal strength,  $f_2$  for the in-plane transverse strength,  $f_{1,s}$  for the in-plane shear strength, and  $f_{2,s}$  for the transverse shear strength. Strength values for tensile (T) and compressive (C) actions are given for in-plane strengths.

### 3.2.1. Elastic constants

The determination of the elastic constants summarized in Table 2 was carried out using micromechanical modelling with volume fractions of the constituents established by using the resin burn-off method, as described in [22]. In making the micromechanical modelling calculations, it is assumed that the densities of matrix and E-glass fibres are  $1.1 \text{ g/cm}^3$  and  $2.56 \text{ g/cm}^3$ . The modulus of elasticity for the matrix constituent is assumed to be  $3.2 \text{ kN/mm}^2$  and for the E-glass fibres it is taken as  $72 \text{ kN/mm}^2$ . The constituent Poisson's ratios are assumed to be 0.36 and 0.22, respectively. Using the rule of mixtures approach with the two reinforcing lamina stiffnesses in Table 2 predictions for the elastic constants of the 9.6 mm thick panel are  $E_1 = 25.0 \text{ kN/mm}^2$ ,  $E_2 = 16.7 \text{ kN/mm}^2$ ,  $G_{12} = 4.5 \text{ kN/mm}^2$  and  $\nu_{12} = 0.36$ . The pultruded material consists of alternative reinforcing layer of UD and the TSFM. A leg panel has a balanced lay-up that comprises TSFM1

layer at 1.38 mm thickness, UD1 at 1.93 mm, TSFM2 at 1.42 mm, TSFM3 at 1.39 mm, UD2 at 2.01 mm and TSFM4 at 1.47 mm.

### 3.2.2. Strength

A series of tension and compression coupon tests were conducted using modified test methods. It should be noted that compression strength is given for fullness. Only compression and tension tests using non-standard coupons were conducted at the University of Warwick. The data for shear strength was taken from standard tests conducted by D'Alessandro [25] on identical pultruded material.

*Compressive Strength Tests:* The test rig, shown in Fig. 3, was designed and manufactured at the University of Warwick as a modified version of the apparatus used by Barker and Balasundaram [26], which was later used by Haeberle and Matthews [27]. Some advantages of this set-up as stated by Mottram [28] are the elimination of end effects, no need for end tabs and failure occurs within the gauge length. The test rig was clamped into a load-controlled 40 metric tonne Amsler universal testing machine and specimens were set within the clamps. The load rate was applied at approximately 10 kN/min and ultimate load recorded. Tests were conducted at ambient laboratory temperatures. All specimens failed within the gauge length initially with audible inter-layer splitting followed by an angled shear crack at approximately 45° throughout the cross-section of the coupon. This crack initiated from one of the loaded-face corners and extended through the thickness and was the predominate-failure mode in most coupons. Fig. 4 shows failed specimens; the typical 45° shear cracks can be seen.

The longitudinal (compression) strength for the batch ranges from 280 to 328 N/mm<sup>2</sup>. The transverse strength is found to range from 99 to 153 N/mm<sup>2</sup>. Although the two batches (each of ten specimens) had a relatively high Coefficient of Variation (CoV) of approximately 10%, no value was removed from further analysis since they all lay within the acceptable bounds as determined by the Chauvenet criteria [29]. Table 3 summarizes the average strengths, Standard Deviation (SD) and CoV from testing 10 nominally identical coupons. The mean compressive strengths in both longitudinal and transverse directions determined by testing are seen to be 25% higher than the pultruder's values tabulated in [21].

*Tensile Strength Tests:* A total of ten longitudinal and ten transverse coupons were tested. Tensile tests were conducted using a load-controlled Amsler universal testing machine; the loading was applied at a rate of approximately 10 kN/min. The ultimate load was recorded. Acoustic emissions could be heard prior to ultimate load being attained, especially in the longitudinal

coupons. Ultimate failure was always by fibre rupture across the specimen width. A failed 90° specimen is shown in Fig. 5, with the typical failure mode of rupture across the specimen width.

Table 4 summarizes the results as for compression loading in Table 3. The CoV ranges between 3 and 10%, with the larger batch dispersion in the transverse direction. The mean longitudinal strength in tension at 294 N/mm<sup>2</sup> is 4% lower than the mean compression, whereas the transverse tensile strength is, as expected, much lower, at 63% of the compression mean of 133 N/mm<sup>2</sup>.

*Shear Strength:* D'Alessandro [25] conducted a series of in-plane shear strength tests in spirit of ASTM D5379 (M) [30] using ten longitudinal specimens only. The use of an Iosipescu test fixture was employed with the in-plane strength and in-plane stiffness (for shear modulus) being measured. The procedure and further details on the test set-up are given in [25] and only salient strength and modulus values are given here. It was found that the mean in-plane shear strength is  $f_{1,s} = 90.6$  N/mm<sup>2</sup> with a SD and CoV of 2.8 N/mm<sup>2</sup> and 3.1%, respectively. The same values are taken for the transverse shear strength ( $f_{2,s}$ ) in this work. The shear stress against shear strain relationship is nonlinear throughout to an ultimate shear strain of > 5%. Using the secant gradient between shear strains of 0.02 and 0.06% the mean in-plane shear modulus is determined to be 4.3 GPa, having a relatively high CoV of 17.1%

#### 4. Finite element simulations

The FE study presented next includes a continuum damage model with a cohesive zone approach to modelling of laminate materials. Continuum damage models address the intralaminar failure mechanisms from a global standpoint, whereas if the analyst used individual damage mechanisms they would be homogenized and constructed around a failure criterion. This approach is the least complex and uses the composite lay-up modeller tool within the Abaqus pre-processor to define the individual laminae through a laminate thickness. Each layer is cohesively bonded together to form the lamination with interfaces assumed to have a thickness of  $10^{-3}t_{lay}$ , where  $t_{lay}$  is the thickness of the thinnest layer either side of the interface. Values for  $t_{lay}$  are reported in Section 3. This modelling dimension plays the role of a length scale, and it has been shown that the thickness of the cohesive interface does not affect the model's performance provided its thickness is small enough compared to  $t_{lay}$  [2].

The static analysis of the delamination dominated progressive failure process in a single equal leg-angle cleat under tensile (tying force) loading is examined and the predictions are compared

with experimental results taken from [4]. The dominant failure mechanism as the cleat progressively fails in testing is delamination cracking, although fibre breakage is observed to occur, and this depends on localized stresses and fibre architecture.

#### 4.1. Description of the model

Figs. 6a and 6b show the dimensions of the cleat problem from [4] that is to be represented and analysed. Each leg of 9.6 mm thickness is 75 mm long and at the junction between the two orthogonal legs there is a fillet radius with inner radius,  $R$ , of 9.6 mm ( $= t$ ). The width of the cleat is 128 mm, and at 32 mm from the 75 mm edges a leg has a M16 steel bolt that give fixity to the vertical displacement boundary condition. There are therefore two bolts across the cleats width. Because of symmetry the modelling adopts half symmetry and the FE mesh has a width of 64 mm. The layers are oriented with their  $0^\circ$  direction coincident with direction of pultrusion. The steel bolting is not explicitly modelled in order to simplify the modelling methodology. Although the bolt restraining action plays an important role in the evaluation of the stiffness of the structural response it is deemed unlikely to have an influence on the load-carrying resistance of the cleat, which is presented below.

The FE model is built-up from stacked continuum shell elements with the individual UD and TSFM layers in Fig. 6b being modelled separately. These elements have the geometry of bricks but their kinematic and constitutive behaviour are similar to those of conventional shell elements. The continuum shell elements are able to reproduce reliable results in simulations of thin-walled structures by means of only one element in a lamina thickness, owing to a higher-order displacement field [31,32]. Cohesive interface elements are used to connect a TSFM and an UD layer to allow for (multi-)delamination failure to occur. As illustrated in Fig. 6b four cohesive interfaces I1 to I4 are considered; there is no such interface required between the two touching TSFM layers at mid-thickness. The in-plane mesh geometry for the interfaces is the same as that for the laminae. The FE mesh specification in our principal study has a total of 85760 continuum shell SC8R elements, and 68608 COH3D8 cohesive elements, and its overall refinement is shown in Fig. 6c.

A monotonic loading for the tensile tying force is applied in the form of an applied uniform vertical displacement  $\delta$  as shown in Fig. 6a. The numerical analysis is performed using a global stabilization factor (dissipated energy fraction) of  $2 \times 10^{-4}$ .

The Abaqus analysis is run with the material properties from Tables 2-4 assigned to the appropriate layers. The Hashin failure criterion [33] is used to predict damage onset and the governing failure mode within each lamina.

The interfacial strength properties were reduced from those of the matrix material by adopting a weakening factor  $f_w$ , according to Puck's guidelines [34, 35]. It was found by a sensitivity analysis that the overall response for  $f_w$  equal to 0.3 gives the one closest to the experimental results in [4], which indicates a relatively weak interface in the pultruded GFRP material. The piecewise linear traction-separation law of the cohesive elements is described according to the mechanical properties of the UD layer presented in the second column in Tables 2 and 4. Using the guidance from Camanho *et al.* [13] the elastic stiffness (per unit area) of the interface is assumed to be equal to  $10^6$  N/mm<sup>3</sup>. The critical normal interface tractions of the cohesive zone elements is equal to the tensile normal strength of the UD layers in direction normal to the fibres,  $f_{2,T}$ , times the weakening factor. The critical shear interface tractions is equal to the shear strength of the UD,  $f_{2,S}$ , times the same weakening factor. Mode I, mode II and mode III critical energy release rates,  $G_{I,c}$ ,  $G_{II,c} = G_{III,c}$ , were taken as 0.2 and 0.5, respectively, for the pultruded material [2].

#### 4.2. Modelling strategy verification

Results from the FE modelling strategy for the static analysis of curved laminates is compared with (plane strain) numerical results taken from the literature [36]. The laminate lay-up arrangement is that of the fifteen layer cross-ply laminate [0/90/0/ ... /0/90/0]. The curved leg-angle section investigated by Wimmer *et al.* [36] has dimensions 11.2×11.2×2.25 mm (for  $t_{lay} = 0.15$  mm) and the internal radius of curvature  $R$  is 2.55 mm. The composite material has laminae with an epoxy resin matrix and a UD reinforcement of carbon fibre. The lamina mechanical properties for the current FE analysis are taken from [36] and summarized in Table 5. Note that with  $f_w = 0.9$  the interface bond is strong. A unit horizontal displacement is prescribed at the top of the 'vertical' leg in order to simulate flexure for the opening mode; that is the angle between the two orthogonal legs is forced to be  $> 90^\circ$ .

Numerical results from Wimmer *et al.* [36] have shown that the critical location for delamination initiation is the interface between layers five and six (going into the 15 layer laminate from the top surface having the smallest fillet radius). As a result of this finding only this particular interface, for a single delamination failure surface, is included in the authors' FE modelling. This approach was used in order to reduce the computational size of this benchmark study.

The leg-angle's strength, here expressed in terms of applied horizontal load per unit length of the laminate, is reached as a result of excessive delamination at the critical interface between the fifth and sixth layers. Fig. 7 is for a plot of strength versus the top horizontal displacement from Abaqus outputs using the Section 3 FE modelling methodology. Maximum load, given by the filled circle symbol, is compared with the FE maximum 'load' prediction of 25.1 N/mm by Wimmer *et al.* [36], which is shown by the horizontal dashed solid line. The authors' nonlinear analysis shows an elastic response to a strength value of 23.7 N/mm, at which there is a sudden reduction to 15.8 N/mm. Further increase to the horizontal displacement shows a slight nonlinear increase in the force that can be resisted. The maximum 'load' predictions are in good agreement (authors' is 6% lower). This finding is not unexpectedly as both represent acceptable numerical formulations to the structural engineering problem. The very acceptable correlation provides a validation for the Abaqus modelling methodology described in Section 3.

Plotted in Fig. 8, on the top surface of the leg-angle, is the delamination damage parameter for the critical interface at the maximum 'load' of 23.7 N/mm. Damage progression can be tracked, from 0 (none) to 1 (complete), using the Abaqus output parameter Stiffness DEgradation, SDEG. The plot used three colours, with blue for undamaged ( $< 0.3$ ), green for partially damaged (0.3 to 0.7) and red ( $> 0.7$ ) for completely damaged. Delamination failure initiates at the leg's junction, in the curved part of the 2.25 mm thick laminate, and propagates into the legs. This leads to a change of the structural stiffness and a reduction of the 'strength' required for a constant horizontal displacement as seen in Fig. 7, indicating that the growth of delamination failure is unstable.

#### 4.3. Analysis results for Pultruded GFRP cleat

Fig. 9 is for a plot of tying force load against applied vertical displacement,  $\delta$ , for the pultruded cleat of size 75×75×9.6 mm (and  $R/t = 1$ ) with loading and displacement boundary conditions defined in Fig. 6a. On the solid line giving the tensile force vs.  $\delta$  relationship there are three points labelled A to C. To point B the relationship is virtually linear. At a load of 8.5 kN (point A), the Abaqus analysis predicts that delamination failure starts to accumulate in a small region over interface I4, which is between layers UD2 and TSFM4 (labelled in Figs. 6b). This level of tying force corresponds to 85% of the maximum of 10 kN, which is point B. After the cleat's resistance has been reached, unstable delamination crack growth takes place on interface I4 localized to the curved region in the laminate. Note that the other three interfaces I1 to I3 remain intact and thereby undamaged (and intralaminar damage does not occur). The progressive damage leads to a considerable increase in the size of delamination, and a consequent drop, to Point C, in the tensile

force that is resisted. Figure 10 has a similar content to Fig. 8, with its parts a) to c) showing the damage states at points A to C in Fig. 9, respectively. Figures 10a and 10b show where delamination starts (point A load) and develops when the ultimate strength at point B is achieved. Figure 10c illustrates the delamination damage that has grown along interface I4 into the horizontal leg, predominantly by the opening mode I illustrated in Fig. 1a.

Presented as constant tying forces in Fig. 9 are two results from the series of tests by Qureshi *et al.* [4]. The horizontal thick line with short dashes at 6.2 kN is for the test load when a change in initial stiffness was recorded. This can be identified as a test signal for the onset of cleat failure by delamination. A noticeable drop of stiffness was observed experimentally, but it is not observed in the numerical predictions plotted in Fig. 9. The horizontal thick line with long dashes at 9.8 kN is for the ultimate (tying force) strength. This experimental result (representing a single cleat) is established from the mean of six cleats, tested in pairs as a standard web-cleated detailing for a simple frame joint [4]. With a 2% difference between the test strength and point B it is observed that there is very good correlation for a pultruded cleat's resistance between the FE simulation and the experimental approach employed by Qureshi *et al.* [4].

#### 4.4. Influence of leg junction on tying resistance

Having demonstrate with two benchmark examples in Sections 4.2 and 4.3 that the FE modelling methodology in Section 3 is effective and reliable it was decided to simulate a tying force problem that cannot be readily characterized by physical testing. Keeping  $t$  constant at 9.6 mm a change in the radius of curvature given by  $R/t = 0.2$  (i.e.  $R = 1.92$  mm) was computationally investigated. By having a much smaller  $R$ , the tying resistance is predicted to increase by 10% to 11 kN. Delamination now initiates at the same interface I4 when the tying force is 7.5 kN, corresponding to about 70% of the maximum load (and 12% lower than when the radius of curvature is generous for  $R/t = 1.0$ ). For the  $R/t = 0.2$  dimensioning it was found that at 10.6 kN delamination cracking starts to emerge in interfaces I2, which as Fig. 6b shows lies between the internal UD1 and the middle TSFM layers. Delamination growth then continues to propagate over both interfaces localized to the curved region in the cleat.

This preliminary result could be for the start of a numerical parametric sensitivity analysis to establish what is an optimum cleat shape and lay-up (dependent on composite processing method) for the strongest cleat against a minimum cost requirement when the governing mode of failure is caused by a tensile tying force.



## 5. Summary and concluding remarks

This paper describes a preparatory FE investigation into the effect of curvature on the resistance of laminate composite structures that fail by initiation and excessive delamination cracking. The effective utilization of thick laminated, curved structural components with out-of-plane loading requires that a methodology for their detailed design be in hand. FE procedures are proposed in this numerical study for the structural analysis, using the general purpose software Abaqus, without user subroutines, to create a model using stacked shell continuum and cohesive zone elements. As recently suggested by Lopes *et al.* [37], a possible sophistication in the FE model methodology is to employ cohesive surfaces to address the delamination failure phenomenon.

In this numerical work, a FE three-dimensional model was developed for calculating the tying force resistance of an equal leg-angle when the loading is out-of-plane of a laminated panel leg. The reliability of the outputs was evaluated by comparing the authors' numerical predictions with other FE results and, importantly, with published results from series of physical tests. In both cases the agreement is shown to be very acceptable given the inherent uncertainties in how the various results have been obtained. It is hoped that the new knowledge and understanding presented in this paper will spur more research into this important structural engineering response and provide insight that will assist in direct future research and design code development endeavours, such as those now transforming the ASCE pre-standard [18] into a published standard with consensus design procedures for pultruded frame construction. It is worthy of mention that currently [18] requires web cleats [4] in simple frame joints to be of steel material because there is a lack of knowledge and understanding towards the performance of composite cleat components, especially over the full service working life (say 50 years) of pultruded structures.

## Acknowledgments

This paper was partially produced in the framework of the project *Structural joints for building frames of pultruded fibre reinforced polymers*. This research was supported by a Marie Curie Intra European Fellowship within the 7<sup>th</sup> European Community Framework Programme under contract grant PIEF-GA-2012-327142. The authors would like to thank Dr. Jawed Qureshi of the University

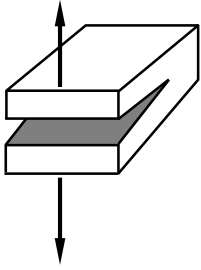
of East London for providing raw test results from a series of tying force tests [4] when he was with University of Warwick.

## References

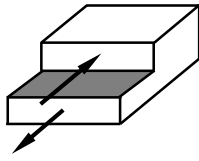
- [1] Mottram JT. Does performance based design with fibre reinforced polymer components and structures provide any new benefits and challenges? *The Structural Engineer* 2011; 89(6):23–27.
- [2] Girão Coelho AM. Finite element guidelines for simulation of delamination dominated failures in composite materials validated by case studies. *Arch Computat Methods Eng* 2015; DOI: 10.1007/s11831-015-9144-1.
- [3] Turvey GJ, Wang P. Failure of pultruded GRP angle-leg junctions in tension. *Proc. 17<sup>th</sup> International Conference on Composite Materials (ICCM17)*, 27-31 July 2009, paper A1:1.
- [4] Qureshi J, Mottram JT, Zafari B. Robustness of simple joints in pultruded FRP frames. *Structures* 2015; 3:120–129.
- [5] Abaqus [Computer Software]. (2015). Version 6.14 Dassault systems, <http://www.3ds.com/products-services/simulia/products/abaqus>.
- [6] CEN (European Committee for Standardization). Actions on structures, part 1.7: General actions – Accidental actions.” *EN 1991-1-7:2006 Eurocode 1*, Brussels, 2006.
- [7] SEI/ASCE (Structural Engineering Institute of the American Society of Civil Engineers). Minimum design loads for buildings and other structures. *SEI/ASCE 7-05*, Reston, VA, USA, 2005.
- [8] Dugdale DS. Yielding of steel sheets containing slits. *J Mech Phys Solids* 1960; 8:100–104.
- [9] Barenblatt GI. The mathematical theory of equilibrium cracks in brittle fracture. *Advances in Applied Mechanics* 1962, HL Dryden, Th von Kármán, G Kuerti, FH van den Dungen, L Howarth, eds.; 7:55–129.
- [10] Ortiz M, Pandolfi A. Finite-deformation irreversible cohesive elements for three dimensional crack-propagation analysis. *Int J Numer Meth Eng* 1999; 44:1267–1282.
- [11] Brewer JC, Lagace PA. Quadratic stress criterion for initiation of delamination. *J Compos Mater* 1988; 22:1141–1155.
- [12] Mohammadi S, Owen DRJ, Peric D. A combined finite/discrete element algorithm for delamination analysis of composites. *Finite Elem Anal Des* 1998; 28:321–336.

- [13] Camanho PP, Dávila CG, Moura MF. Numerical simulation of mixed-mode progressive delamination in composite materials. *J Compos Mater* 2003; 37(16):1415–1438.
- [14] Benzeggagh ML, Kenane M. Measurement of mixed-mode delamination fracture toughness of unidirectional glass/epoxy composites with mixed-mode bending apparatus. *Compos Sci Technol* 1996; 56:439–449.
- [15] Falk ML, Needleman A, Rice JR. A critical evaluation of cohesive zone models of dynamic fracture. *J Phys IV* 2001; Proc 11(Pr.5):43–50.
- [16] Turon A, Dávila CG, Camanho PP, Costa J. An engineering solution for mesh size effects in the simulation of delamination using cohesive zone models. *Eng Fract Mech* 2000; 74:1665–1682.
- [17] Johnson RB, Mahamid M. Design of steel connections for tie forces. ASCE Structures Congress. ASCE Structures Congress 2010, Orlando, Florida, USA; 943–954. DOI: 10.1061/41130(369)86.
- [18] ASCE (American Society of Civil Engineers). Pre-Standard for Load & Resistance Factor Design (LFRD) of Pultruded Reinforced Polymer (FRP) Structures, Arlington, VA, USA, 2010.
- [19] Bank LC. Composites for construction: Structural design with FRP materials, John Wiley & Sons, New Jersey, USA, 2006.
- [20] Starr T. Pultrusion for engineers, Woodhead publishing Ltd., Cambridge, UK, 2000.
- [21] Creative Pultrusions. The new and improved Pultrex<sup>®</sup> pultrusion design manual, Creative Pultrusions Inc., Alum bank, PA, USA, 2010.
- [22] Lane A. An experimental investigation of buckling mode interaction in PFRP columns, PhD thesis, University of Warwick, UK, 2002.
- [23] ASTM (American Society for Testing and Materials). Standard test method for ignition loss of cured reinforced resins. *D2584-11*, West Conshohocken, Pennsylvania, USA, 2011.
- [24] Ye BS, Svenson AL, Bank LC. Mass and volume fraction properties of pultruded glass fibre-reinforced composites. *Composites* 1995; 26(10):725–731.
- [25] D'Alessandro RG. Characteristic values of mechanical properties of wide-flange pultruded FRF beams, MSc Thesis, University of Wisconsin-Madison, USA, 2009.
- [26] Barker AJ, Balasundaram V. Compression testing of carbon fibre reinforced plastics exposed to humid environments. *Composites* 1987; 18(3):217–226.
- [27] Haeberle J, Matthews FL. Studies on compressive failure in unidirectional CFRP using an improved test method. Proc. 4<sup>th</sup> European Conference on Composites (ECCM-4) 1990, European Association for Composite Materials, Elsevier, London, UK, 517–523.

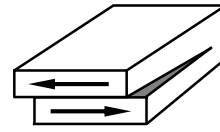
- [28] Mottram JT. Compression strength of pultruded flat sheet material. *J Mater Civ Eng* 1994; 6(2):185–200.
- [29] Kennedy JB, Neville AM. *Basic statistical methods for engineers and scientists*, 3<sup>rd</sup> Edition, Harper & Row, London and New York, 1986.
- [30] ASTM (American Society for Testing and Materials). Standard test method for shear properties of composite materials by the V-notched beam method. *D5379/D5379M-12*, West Conshohocken, Pennsylvania, USA, 2012.
- [31] Parisch H. A continuum-based shell theory for non-linear applications. *Int J Numer Meth Eng* 1995; 38:1855–1833.
- [32] Remmers JC, Wells GN, de Borst R. A solid-like shell element allowing for arbitrary delaminations. *Int J Numer Meth Eng* 2003; 58:1701–1736.
- [33] Hashin Z. Analysis of composite materials. *J Appl Mech* 1983; 50:481–505.
- [34] Knops M. Analysis of failure in fiber polymer laminates – the theory of Alfred Puck. Springer, Germany, 2008.
- [35] Puck A, Schürmann H. Failure analysis of FRP laminates by means of physically based phenomenological models. *Compos Sci Technol* 2002; 62:1633–1662.
- [36] Wimmer G, Schuecker C, Pettermann HE. Numerical simulation of delamination in laminated composite components – A combination of a strength criterion and fracture mechanics. *Compos Part B-Eng* 2009; 40:158–165.
- [37] Lopes CS, Sádaba S, González C, Llorca J, Camanho PP. Physically-sound simulation of low-velocity impact on fibre reinforced laminates. *Int J Impact Eng* 2015; DOI: 10.1016/j.ijimpeng.2015.05.014



**a)** Mode I ( $m = \text{I}$ ): opening



**b)** Mode II ( $m = \text{II}$ ): sliding



**c)** Mode III ( $m = \text{III}$ ): tearing

**Fig. 1.** Modes of delamination failure

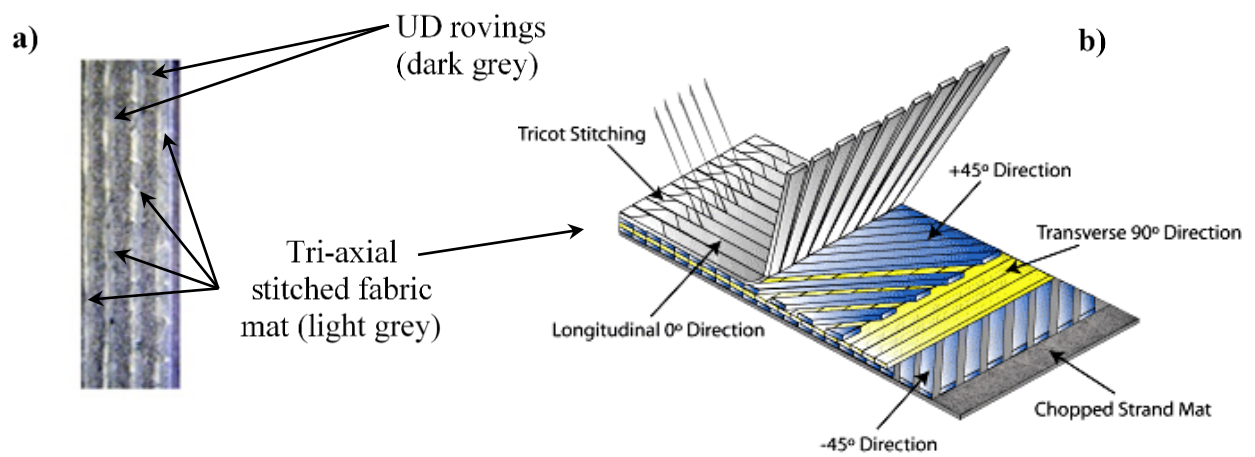


**Fig. 2.** Sections of GFRP composite angle cleats showing **a)** Leg material and **b)** Tri-axial stitched fabric sketch (<http://vectorply.com/stitch-bonded-reinforcements/>)

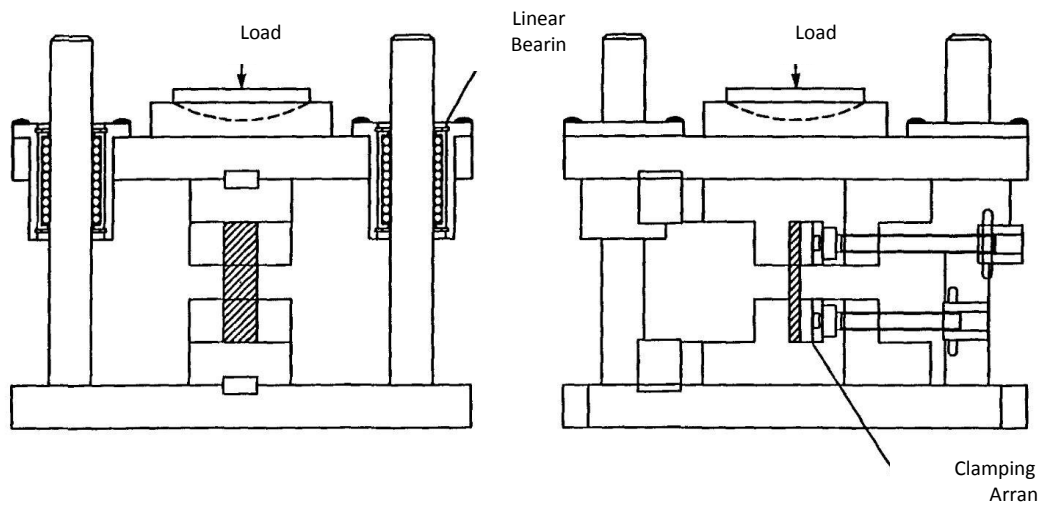
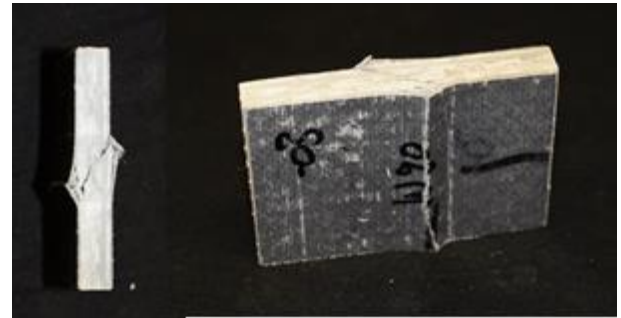


**Fig. 3.** Compression test rig and clamping arrangement drawing [28]



**a)** Material orientated at  $0^\circ$



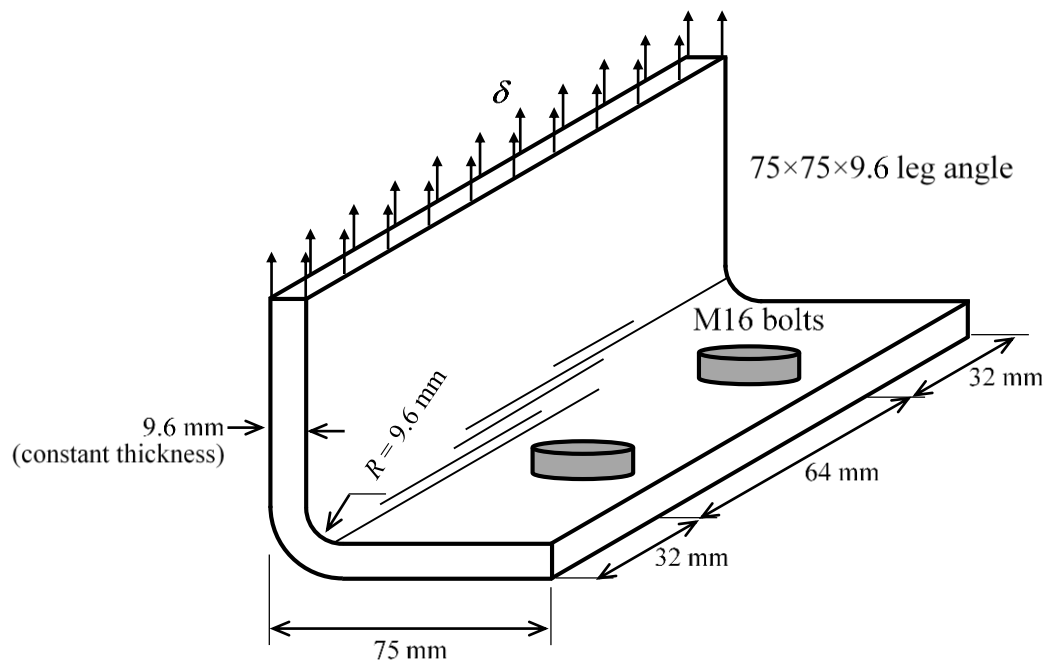
**b)** Material orientated at  $90^\circ$

**Fig. 4.** Failed compression test specimen

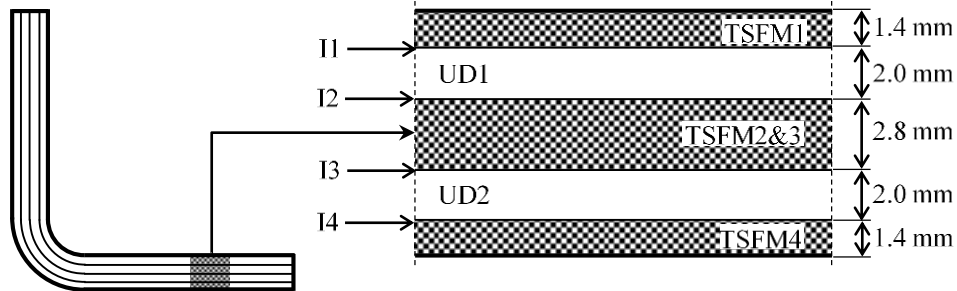




**Fig. 5.** Failed tension test specimen (material orientated at 90°)



a) Schematic of leg-angle with tying force



b) Composite lay-up adopted in the numerical study



c) FE mesh

**Fig. 6.** Composite angle cleat geometry

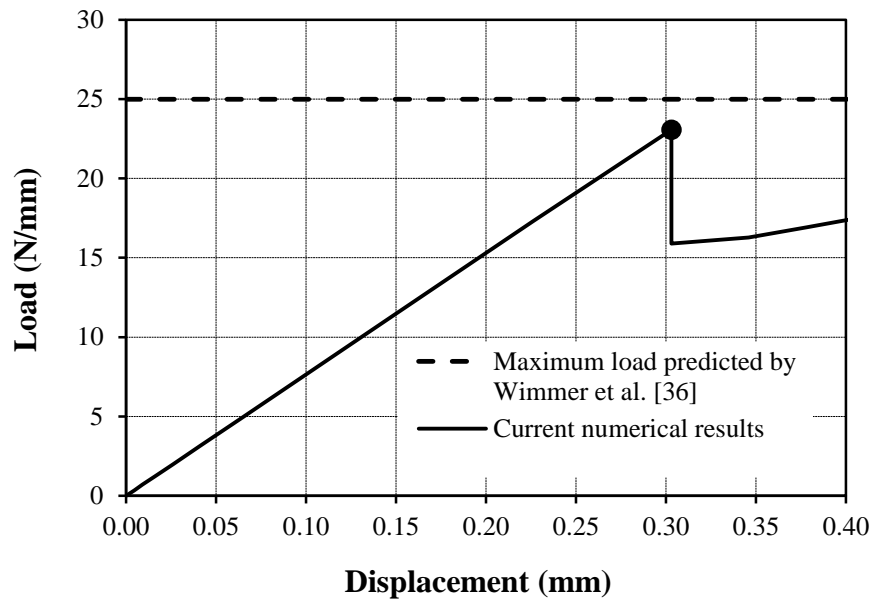


**Fig. 7.** Load-top displacement plot resulting from implementing the current FE model, and comparison with existing numerical data from Wimmer *et al.* [36]

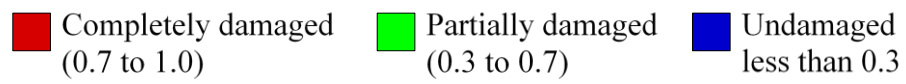
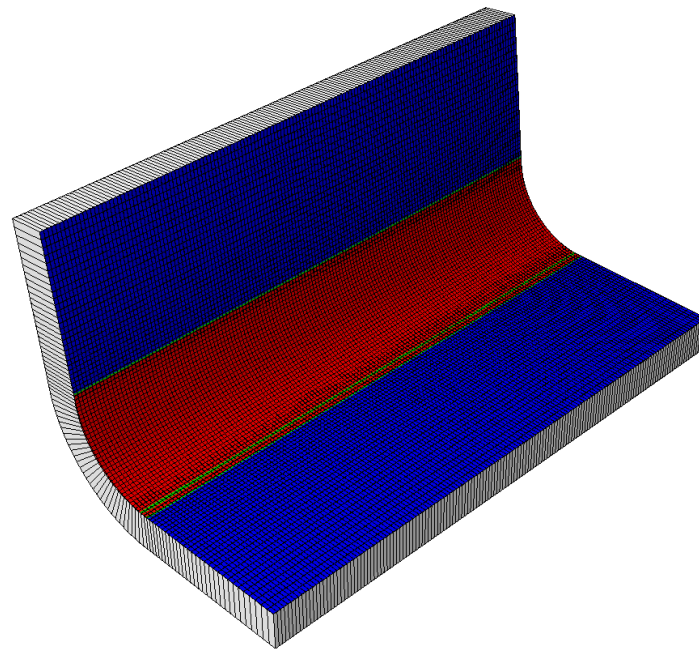


**Fig. 8.** Delamination between layers five and six at maximum predicted load (plots on deformed structure, magnification factor 5)

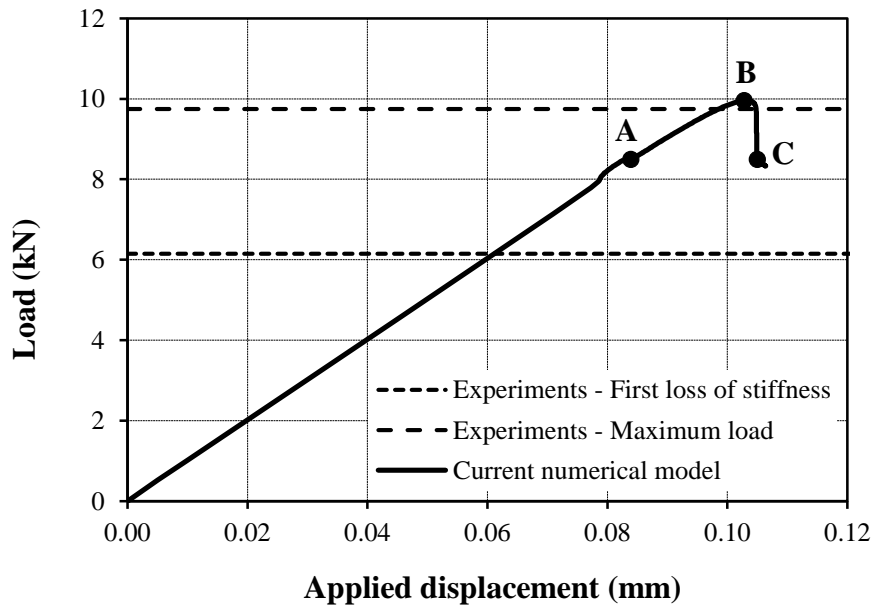
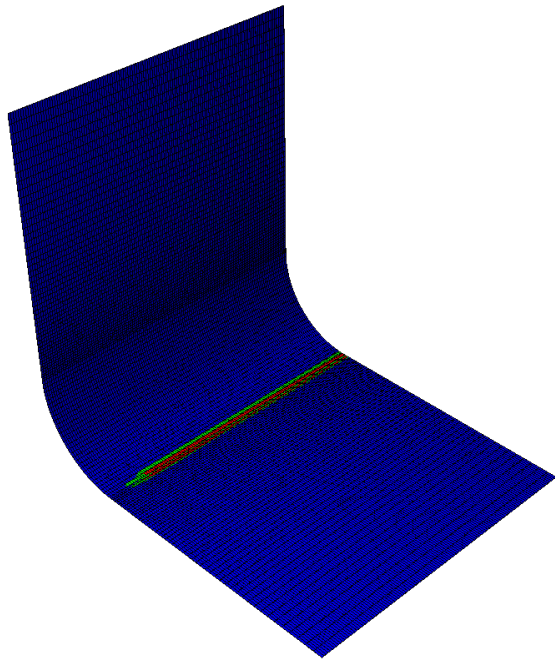
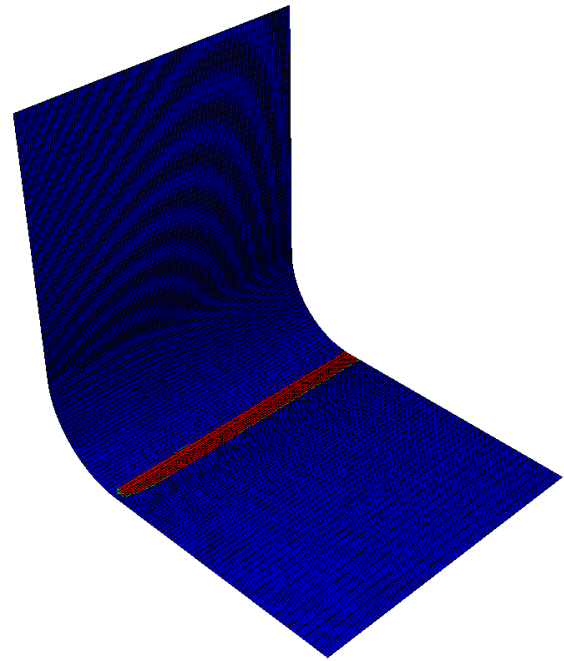


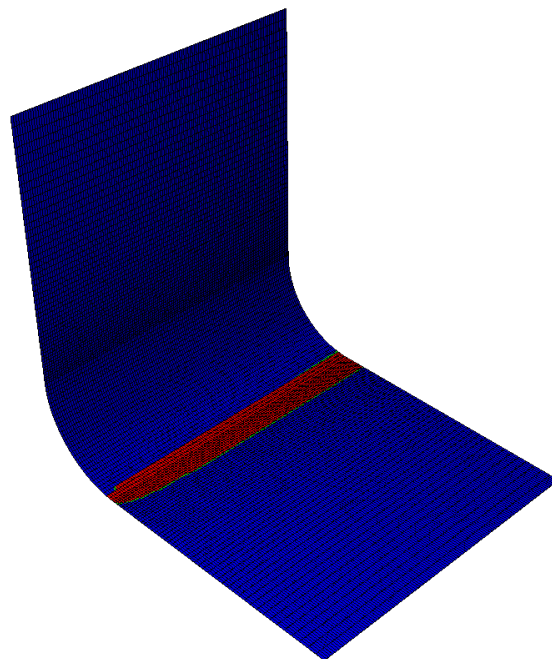
**Fig. 9.** Tensile load-top displacement plot resulting from implementing the current FE model, and comparison with existing numerical data (per cleat) from Qureshi *et al.* [4]



**a)** Onset of delamination damage (point A, Fig. 9)



**b)** Maximum load (point B, Fig. 9);



**c)** Delamination damage propagation (point C, Fig. 9)

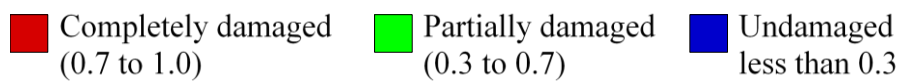


**Fig. 10.** Delamination damage onset and propagation with load at interface I4

**Table 1.** Material constituent properties

	Constituent part			
	SV	TSFM	UD	Matrix
Number of layers in thickness	2	4	2*	—
Fibre architecture	Random fibre veil	+45°/90°/-45°/CSM	156 (56 yield)	—
% volume in total	3	34	33	30
% total of fibre reinforcement	5	48	47	—
Nominal layer thickness (mm)	0.03	1.4	2.0	—

\* There is no UD layer found in between the middle TSFM layers as confirmed from observation of cross-section in Fig. 2a.

**Table 2.** Elastic constants from micromechanical analysis

	Constituent part		
	UD	TSFM	
		Mat layer (+45°/90°/-45°)	CSM
$E_1$ (kN/mm <sup>2</sup> )	44.7	13.1	7.7
$E_2$ (kN/mm <sup>2</sup> )	14.0	25.5	7.7
$G_{12}$ (kN/mm <sup>2</sup> )	4.1	6.1	2.7
$\nu$	0.28	0.41	0.41



**Table 3.** Summary of compression test results (average of a batch of ten tests)

Batch	Compressive strength (N/mm <sup>2</sup> )	SD (N/mm <sup>2</sup> )	CoV (%)
0° (1,C)	306	21.0	6.9
90° (2,C)	133	14.3	10.7

**Table 4.** Summary of tension test results (average of a batch of ten tests)

Batch	Tensile strength (N/mm <sup>2</sup> )	SD (N/mm <sup>2</sup> )	CoV (%)
0° (1,T)	294	7.6	2.6
90° (2,T)	84	8.6	10.0

**Table 5.** Lamina and interfacial properties of the curved laminate analysed by Wimmer *et al.* [36]

Elastic lamina properties		Lamina strength properties		Interfacial properties	
$E_1$ (N/mm <sup>2</sup> )	139300	$f_{1,T}$ (N/mm <sup>2</sup> )	1517	$K_I=K_{II}=K_{III}$ (N/mm <sup>3</sup> )	$3 \times 10^5$
$E_2 = E_3$ (N/mm <sup>2</sup> )	9720	$f_{1,C}$ (N/mm <sup>2</sup> )	1593	$f_I$ (N/mm <sup>2</sup> )	40.5*
$G_{12} = G_{13}$ (N/mm <sup>2</sup> )	5590	$f_{2,T}$ (N/mm <sup>2</sup> )	45	$f_{II} = f_{III}$ (N/mm <sup>2</sup> )	96.3*
$\nu_{12}$	0.29	$f_{2,C}$ (N/mm <sup>2</sup> )	253	$G_{I,c}$ (N/mm)	0.15
		$f_{1,S} = f_{2,S}$ (N/mm <sup>2</sup> )	107	$G_{II,c} = G_{III,c}$ (N/mm)	0.4

\* These values correspond to a weakening factor of 0.9.